

A Novel Anthraquinone-Based Azo Compound: Synthesis, Quantum Chemical Calculations and Investigation of ADMET Properties

Mehmet ULUTÜRK¹, Çiğdem KARABACAK ATAY^{2*}, Bülent DEDE³,
Tahir TİLKİ³

¹ TÜBİTAK Marmara Research Center, 41470, Gebze, Kocaeli, Turkey

² Burdur Mehmet Akif Ersoy University, Faculty of Education, Department of Basic Education,
15030, Burdur, Turkey

³ Süleyman Demirel University, Faculty of Science & Arts, Department of Chemistry,
32260, Isparta, Turkey

(ORCID: [0000-0003-3931-5328](https://orcid.org/0000-0003-3931-5328)) (ORCID: [0000-0001-7226-9971](https://orcid.org/0000-0001-7226-9971))

(ORCID: [0000-0003-1416-7373](https://orcid.org/0000-0003-1416-7373)) (ORCID: [0000-0002-1040-2375](https://orcid.org/0000-0002-1040-2375))



Keywords: Azo, Anthraquinone, DFT, ADMET, Toxicity

Abstract

This study involved the synthesis of the potential drug candidate 2-[(9,10-dioxo-9,10-dihydroanthracen-2-yl) diazenyl]-5-hydroxybenzoic acid (DHA), the elucidation of its structure using spectroscopic techniques, and the determination of the compound's lowest energy structure using the DFT/B3LYP method and the 6-311G(d,p) basis set. The compound's vibration frequencies and NMR chemical shift values were then determined using optimized geometry. The three-dimensional molecular electrostatic potential (MEP) map of the compound and the HOMOs-LUMOs and molecular orbital energies were examined using the DFT approach. The compound's ADMET properties were then determined, and its potential to usage as a drug was assessed. The predicted toxicity class and LD₅₀ value for the DHA were also established. The outcomes demonstrated that by having ADMET properties, this newly synthesized compound has the potential to be a drug.

1. Introduction

Due to their high bioactivity and low toxicity, anthraquinones, which include three benzene rings wherein the keto groups are located on the central ring (9,10-anthracenedione), have been discovered to be fascinating. Due to their biological, pharmacological, and industrial potential, they are receiving greater attention today. For example, they exhibit great enzyme inhibition properties [1]-[3]. In addition to being used as dye pigments in the cosmetics, pharmaceutical, and food sectors [4], [5], its pharmacological potential also includes anticancer, antibacterial, immunosuppressive, antioxidant, antipyretic, diuretic, anti-inflammatory, and antiviral properties [6]-[9]. The compounds should exhibit both strong biological activity and minimal toxicity. In the process of develop-

ing a new drug, it is critical to assess the pharmacokinetic characteristics of newly synthesized compounds. Lipinski's rule of five, also known as the drug-similarity test, establishes the structural characteristics desired in a candidate compound that can be a drug based on the relationship between pharmacokinetic and physicochemical parameters [10]. In silico research thus enables us to understand the likelihood that a chemical may be a potentially good drug [11].

Based on all of this knowledge, a compound with a strong potential to become a drug, 2-[(9,10-dioxo-9,10-dihydroanthracen-2-yl) diazenyl]-5-hydroxybenzoic acid (DHA) based on anthraquinones, was synthesized in our work. One of the factors contributing to the preference for this molecule is the inclusion of azo and anthraquinone groups in its structure. The presence of azo groups in a compound's

*Corresponding author: ckatay@mehmetakif.edu.tr

Received: 08.04.2023, Accepted: 15.08.2023

structure is known to confer highly bioactive characteristics. There have been more studies in recent years on the synthesis of azo-containing compounds and the analysis of their in vitro and in silico characteristics. It is stated that synthesized azo molecules show significant anticancer properties against cancer cells in in vitro studies and even have the potential to become anticancer drugs as a result of in vivo and other studies [12]-[14]. Because of the biological significance of anthraquinones and azo groups in the literature, this study was designed to discover novel potential bioactive chemicals. Spectroscopic techniques were used to clarify its structure. The 6-311G(d,p) basis set and the DFT/B3LYP method were used to perform quantum chemical calculations on the molecule's molecular structure, vibrational spectroscopic data, electronic transition absorption wavelengths, HOMOs and LUMOs analyses, and molecular electrostatic potential (MEP). Absorption, distribution, metabolism, excretion, and toxicity (ADMET) parameters were calculated using the SwissADME and ProTox-II servers.

2. Material and Method

2.1. Physical measurements

Sigma&Aldrich and Merck Chemical Companies provided the chemicals and solvents used in the investigation, which were then used directly without further purification. With the use of a Perkin Elmer Frontier Spectrometer and KBr, FT-IR analysis was carried out. Utilizing a Varian 600 MHz NMR spectrometer, NMR analyses were carried out on deuterated dimethylsulfoxide (DMSO- d_6), and chemical shifts are given in δ units (ppm). On a Shimadzu UV-1800 spectrophotometer, UV-Visible absorption spectra were captured at the wavelength of DHA's maximum absorption (max) in dimethylsulfoxide (DMSO). Acetone was used to produce high-resolution electrospray ionization mass spectra (HR-ESI-MS) on a Thermo Scientific Q Exactive, Orbitrap LC/HRMS system. A BÜCHI Melting Point M-565 equipment was used to determine the melting point in an open glass capillary tube.

2.2. Synthesis of 2-[(9,10-dioxo-9,10-dihydroanthracen-2-yl) diazenyl]-5-hydroxybenzoic acid (DHA)

An ice-salt bath was used to cool a solution of 558 mg (2.5 mmol, 1.00 eq) 2-aminoanthraquinone in 5 mL of concentrated HCl and 3 mL of water to (-5)-0 °C. Next, a cold solution of NaNO₂ (190 mg, 2.75 mmol, and 1.10 eq) in 2 mL of water was added dropwise while being constantly stirred. The diazonium salt was produced when the mixture was agitated for an hour at a temperature of 0 °C or lower. The freshly-prepared anthraquinonediazonium salt was slowly added into the solution of *m*-hydroxybenzoic acid (345 mg, 2.5 mmol, 1.00 eq) in saturated NaHCO₃ a.q. (150 mL) at 0-5 °C. The reaction mixture was stirred for 4 h at 0-5 °C. After adding 1M HCl solution to the resulting dark brown solution to bring the pH level to 4-5, 100 mL of ice water was added. The mixture was stirred for 1 hour at 5 °C. The precipitated material was removed through filtering, washed with cold water, and then recrystallized using a 1:1 solution of ethanol and water before being dried at 50 °C under vacuum. 2-[(9,10-dioxo-9,10-dihydroanthracen-2-yl)diazenyl]-5-hydroxybenzoic acid, (DHA) was obtained 720 mg as brown solid, yield is %77. **Figure 1** illustrates the synthetic method for producing DHA. **Mp** 251-253 °C; **FT-IR** (KBr): ν_{\max} (cm⁻¹) = 3066, 2673, 1716, 1674, 1587, 1572, 1466, 1429, 1326, 1291, 1223, 1169, 1127, 1068, 982, 931, 896, 848, 839, 808, 780, 724, 708, 657, 635, 595, 571, 485, 471, 454; **¹H-NMR** (600 MHz, DMSO- d_6): δ = 13.02 (br, s, 1H), 11.30 (br, s, 1H), 8.38 (d, *J* = 2.2 Hz, 1H), 8.31 (d, *J* = 8.2 Hz, 1H), 8.19-8.14 (m, 3H), 7.91-7.88 (m, 2H), 7.73 (d, *J* = 8.7 Hz, 1H), 7.08 (d, *J* = 2.8 Hz, 1H), 7.03 (dd, *J* = 8.8, 2.6 Hz, 1H); **¹³C-NMR** (150 MHz, DMSO- d_6): δ = 182.0, 181.8, 168.5, 161.5, 154.9, 142.2, 136.0, 134.7, 134.6, 134.5, 134.3, 133.7, 133.2, 133.1, 128.6, 127.7, 126.8, 119.9, 119.7, 117.9, 114.8; **HR-ESI-MS** (C₂₁H₁₂N₂O₅ Exact Mass: 372.07462): calcd for [M + H]⁺ : 373.08190, found: 373.07877 (**Figure 2**); **UV-VIS** (DMSO): λ_{\max} (Abs.) = 342 nm (1.723), 390 nm (2.161).

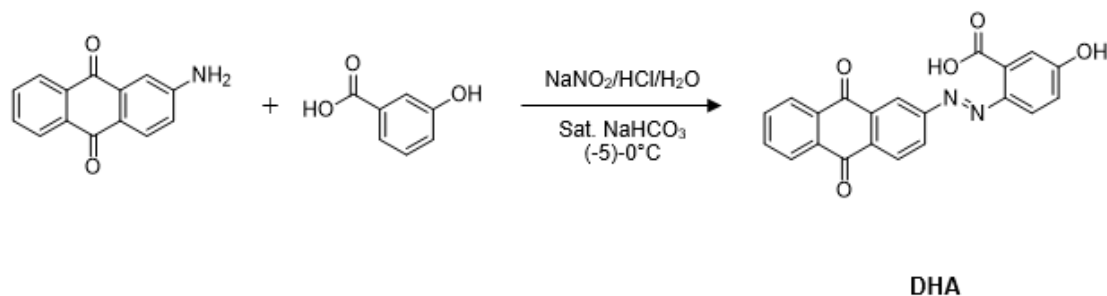


Figure 1. Synthesis of the DHA

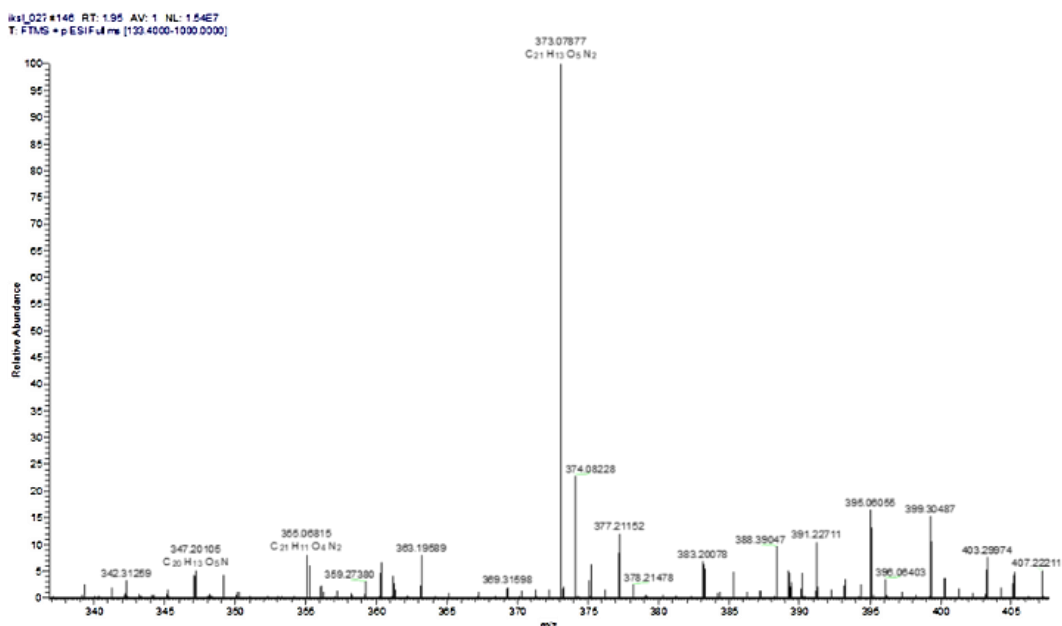


Figure 2. Experimental HR-ESI-MS spectrum of the DHA

2.3. Computational methods

Calculations for quantum chemistry were performed using the Gaussian 09 package, and visualizations were done using the GaussView 5.0.9 program [15], [16]. The molecular structure of the DHA in the ground state was calculated using the DFT method and the B3LYP functional with the 6-311G(d,p) basis set [17], [18]. Additionally, vibrational wavenumbers at the DFT/B3LYP/6-311G(d,p) level were determined. In order to avoid systematic mistakes, the calculated vibrational wavenumbers for the B3LYP/6-311G(d,p) basis set were scaled as 0.9682 for frequencies greater than 1700 cm⁻¹ and 1.0119 for frequencies less than 1700 cm⁻¹ [19]. The same basis set and B3LYP level of the time dependent density functional theory (TD-DFT) were used to model UV-vis spectra [20], [21]. The excitations' contribution rates were computed with GaussSum 3.0 [22]. To find the

shielding factors for ¹H, and ¹³C-NMR, the gauge-invariant atomic orbital (GIAO) method was used [23], [24].

2.4. ADMET predictions

The SwissADME web server calculated ADME characteristics for the DHA, including its physicochemical, pharmacokinetic, lipophilicity, and drug similarity [25]. Using the ProTox-II web server, the toxicity profile, LD50 value, and acceptable use range of DHA were discovered [26].

3. Results and Discussion

3.1. NMR spectra

The ¹H- and ¹³C-NMR chemical shifts of the DHA were determined using the Gauge-Independent Atomic Orbital (GIAO) method at DFT/B3LYP/6-311G(d,p) level.

While its estimated chemical shift was determined to be 5.10 ppm, the O-H group proton H40 was found to be a singlet signal at 11.30 ppm. Although the carboxylic acid proton H39 was empirically detected as a singlet peak at 13.02 ppm, the DFT method calculated its value to be 5.90 ppm. In the expected region, aromatic protons were discovered. They were meant to be in the range of 7.04-8.79 ppm in theory,

but they were actually measured empirically to be in the range of 7.03-8.38 ppm. For ease of comparison between the experimental and predicted chemical shift values of the DHA, $^1\text{H-NMR}$ values were given collectively in **Table 1**. In **Figures 3** and **4**, experimental and calculated $^1\text{H-NMR}$ spectra for the substance were displayed.

Table 1. Experimentally and theoretically obtained $^1\text{H-NMR}$ chemical shifts

H Number	Experimental	Theoretical
H35	7.73	8.79
H33	8.38	8.69
H31-H32-H34	8.19-8.14	8.52
H36	8.31	8.30
H29-H30	7.91-7.88	8.04
H37	7.03	7.40
H38	7.08	7.04
H39	13.02	5.90
H40	11.30	5.10

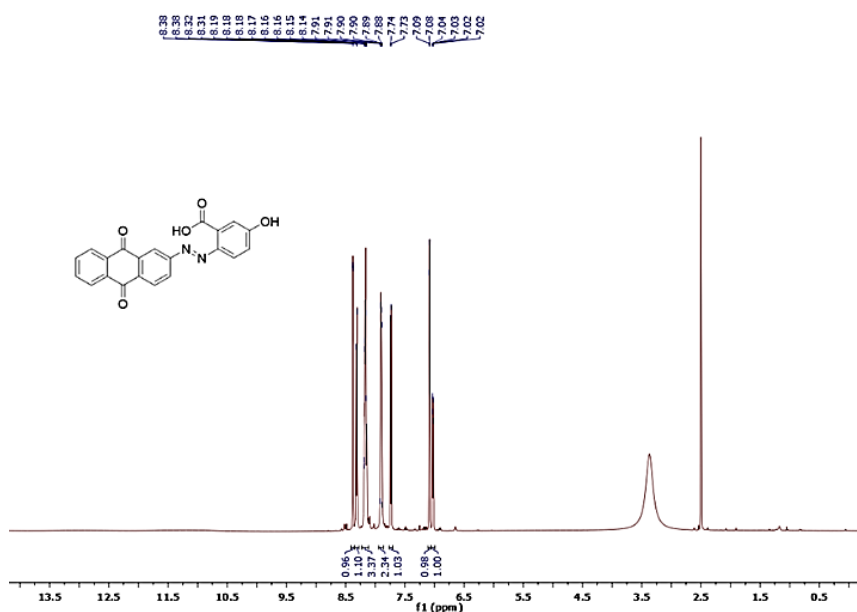


Figure 3. Experimental $^1\text{H-NMR}$ (DMSO-d₆) spectrum of the DHA

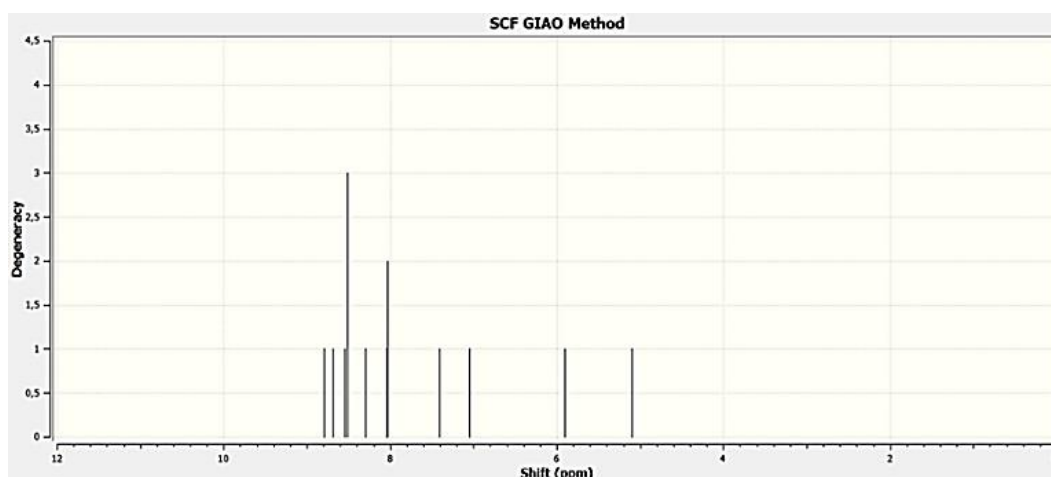


Figure 4. Theoretical ^1H -NMR (DMSO- d_6) spectrum of the DHA

In the ^{13}C -NMR spectrum, the C22 atom associated with the O-H group was measured and logged at 161.5 ppm, while this signal was discovered at 166.4 ppm in the theoretical spectrum. The carboxylic acid group's carbon atom C25 was correlated with a signal at 168.5 ppm, and their computed chemical shift was visible at 174.1 ppm. The results are detailed

in **Table 2**, and all other carbon atoms were found in the predicted area. In **Figures 5** and **6**, the compound's experimental and computed ^{13}C -NMR spectra were displayed.

Table 2. Experimentally and theoretically obtained ^{13}C -NMR chemical shifts

C Number	Experimental	Theoretical
C10	182.0	186.6
C7	181.8	185.9
C25	168.5	174.1
C22	161.5	166.4
C13	154.9	158.9
C19	142.2	151.2
C12	119.9	142.3
C20	127.7	140.6
C2	133.7	139.4
C1	134.3	139.2
C8	134.7	137.9
C9	136.0	137.6
C5	134.6	137.0
C4	134.5	136.9
C11	126.8	133.4
C6-C3	133.1	131.6
C24	117.9	127.2
C21	119.7	121.2
C23	114.8	120.7
C14	128.6	115.3

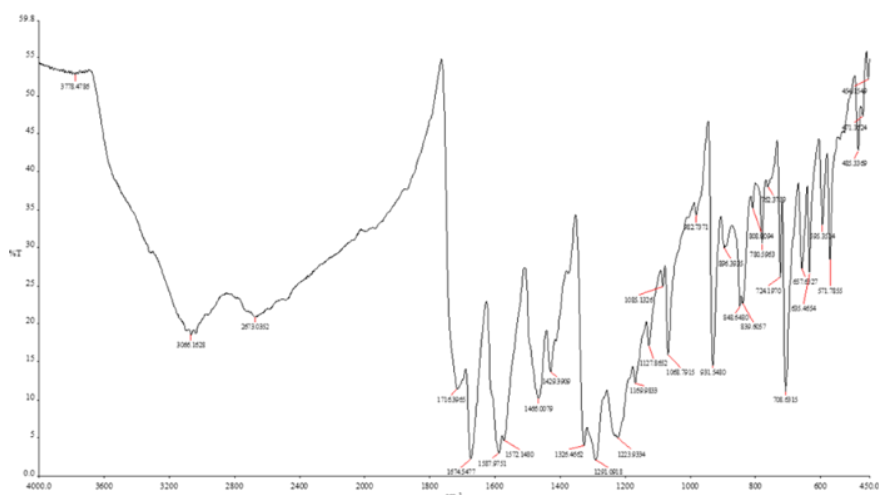


Figure 7. Experimental FT-IR spectrum of the DHA

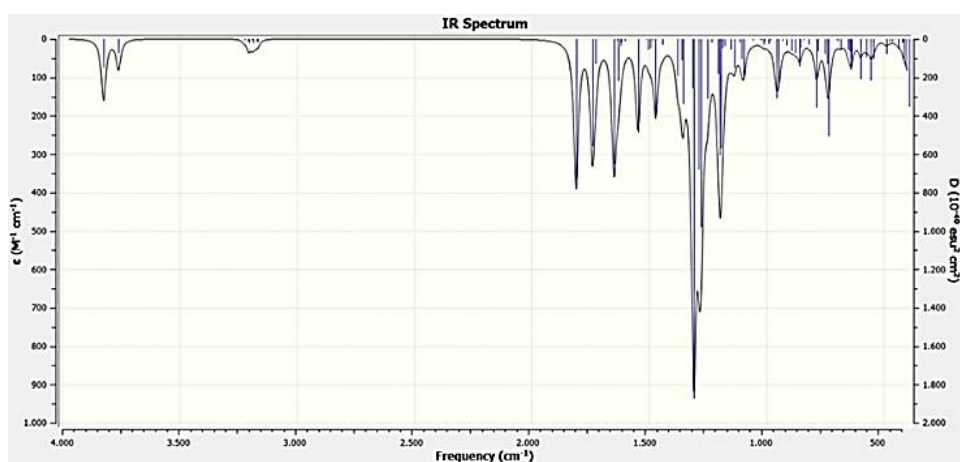


Figure 8. Theoretical FT-IR spectrum of the DHA

3.3. UV-vis spectrum and frontier molecular orbitals

Between 300 and 600 nm, the UV-vis spectra of DHA in DMSO were recorded. The electronic transition wavelengths of the DHA were computed using the TD-DFT technique and the B3LYP/6-311G (d,p) level. **Figures 9** and **10** represent the experimental and theoretical UV-vis spectra of the compounds, respectively. The experimental UV-vis spectra of the

compound were detected at 390 nm and theoretically calculated to be at 351 nm. This band was caused by the $\pi \rightarrow \pi^*$ transition in DHA and contributed 61% by HOMO \rightarrow LUMO. The other band observed in the experimental spectrum belonged to the $n \rightarrow \pi^*$ transition and was at 342 nm. This band was calculated theoretically at 306 nm and it was determined that the HOMO \rightarrow LUMO+1 transition contributed 49% to this band.

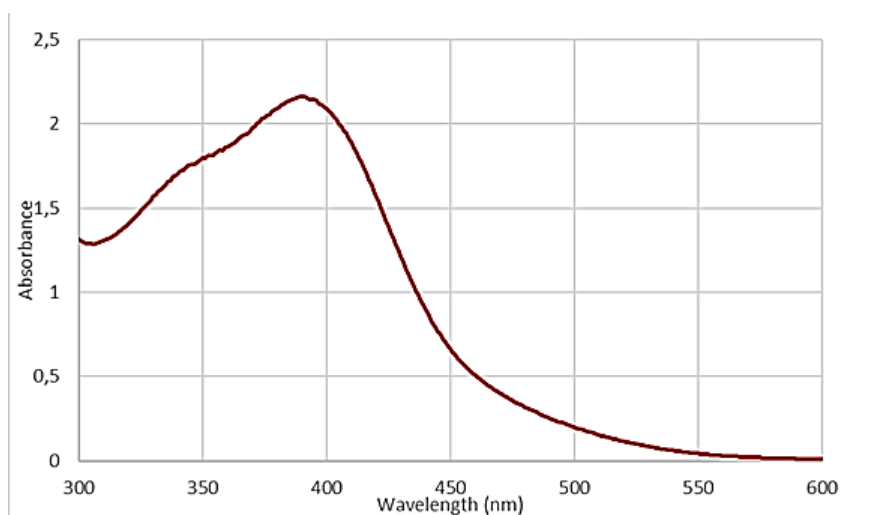


Figure 9. Experimental UV-VIS spectrum of the DHA in DMSO

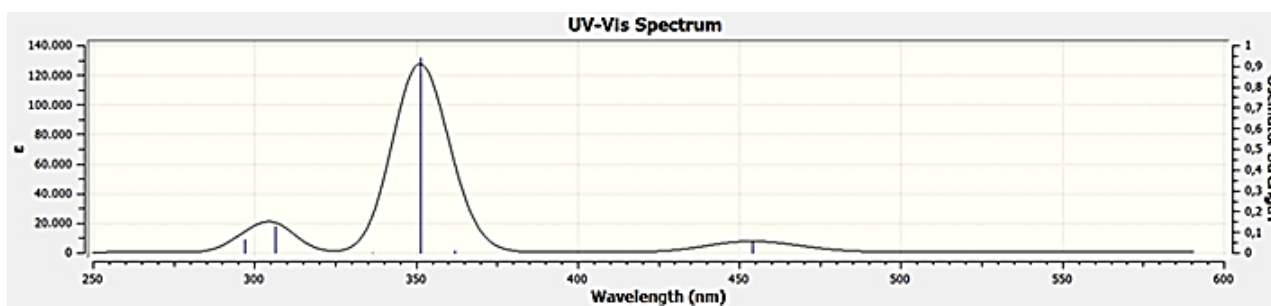


Figure 10. Theoretical UV-VIS spectrum of the DHA in DMSO

When studying the light that is released or reflected when an object is excited, the HOMO-LUMO energy gap offers crucial information about the hardness, softness, stability, and color of the compounds. The HOMOs and LUMOs of the DHA were calculated at the B3LYP/6-311G(d,p) level using the DFT method. The molecular orbital surfaces, energies, and energy difference between HOMO and LUMO of the compound were detailed in **Figure 11**.

Analysis of the HOMO-LUMO graph of DHA revealed that HOMOs clustered on the hydroxybenzoic acid moiety, whereas LUMOs clustered on the hydroxybenzoic acid and anthraquinone moieties. The DHA's HOMO and LUMO energies were determined to be -6.461 and -3.212 eV, respectively, and the energy value for the HOMO-LUMO gap was determined to be 3.249 eV.

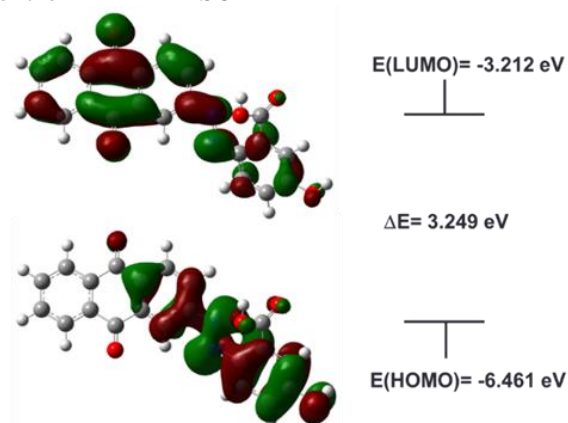


Figure 11. Molecular orbital surfaces, energies, and energy gap between HOMO and LUMO of the DHA

Some of the global reactivity characteristics identified using the HOMO-LUMO energy values of the DHA are shown in **Table 3**. The following electronic factors were created:

$$I \text{ (Ionization Potential)} = -E_{HOMO},$$

$$A \text{ (Electron Affinity)} = -E_{LUMO},$$

$$\chi \text{ (Electronegativity)} = (I + A)/2,$$

$$\eta \text{ (Chemical Hardness)} = (I - A)/2,$$

$$S \text{ (Chemical Softness)} = 1/2\eta$$

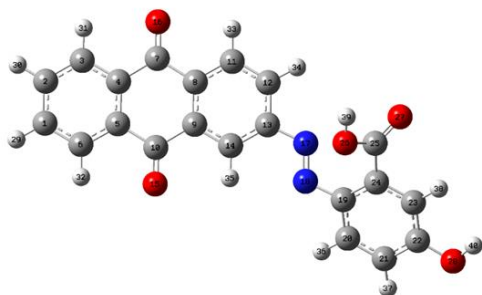
Table 3. Global reactivity descriptors for the DHA

Parameter	Value
E_{HOMO} (eV)	-6.461
E_{LUMO} (eV)	-3.212
ΔE (eV)	3.249
I (eV)	6.461
A (eV)	3.212
χ (eV)	4.836
η (eV)	1.624
S (eV ⁻¹)	0.308

3.4. Computational details

3.4.1. Molecular structure

To achieve the optimized geometry for the DHA, a B3LYP functional with a 6-311G(d,p) basis set was used. The complete optimized geometry of DHA, including atom numbering, is shown in **Figure 12**.

**Figure 12.** Optimized molecular geometry of the DHA calculated at DFT/B3LYP/6-311G(d,p) level

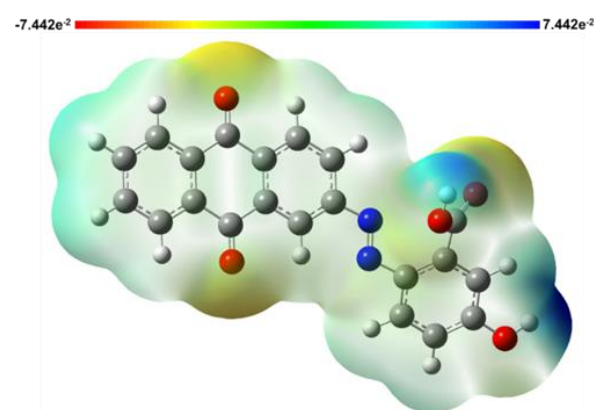
The values for the computed bond lengths (Å), bond angles (°), and dihedral angles (°) were shown in **Table 4**, and according to this, the shortest calculated bond length belonged to the atoms C25 and O27. After comparing the bond angles between the atoms, it was discovered that the C24-C25-O27 bond angle was a little larger. A dihedral angle equal to or close to 0° or 180° indicates that the atoms are in the same plane. C13-N17-N18-C19 had a dihedral angle of 178.4°, which indicated that these units were lying in the same plane.

Table 4. Some selected calculated bond lengths (Å), bond and dihedral angles (°) for the DHA at the B3LYP/6-311G(d,p) level.

Parameters	B3LYP/6-311G(d,p)
Bond lengths (Å)	
N17-N18	1.254
N18-C19	1.405
C22-O28	1.357
C25-O27	1.205
C25-O26	1.350
C7-O16	1.220
C10-O15	1.218
Bond angles (°)	
C4-C7-O16	121.4
C5-C10-O15	121.4
C13-N17-N18	115.0
C24-C25-O27	124.1
N17-N18-C19	114.9
C21-C22-O28	117.6
C24-C25-O26	112.4
Dihedral angles (°)	
C13-N17-N18-C19	178.4
O15-C10-C9-C8	179.5

3.4.2. Molecular electrostatic potential (MEP) diagram

The Molecular Electrostatic Potential (MEP) diagram, which is essential in distinguishing the nucleophilic and electrophilic regions of the molecule, can provide information on the value of the electrostatic potential and the distribution of charges. The MEP maps' red and blue areas, respectively, correspond to the molecule's electronically dense and deficient regions. DFT/B3LYP/6-311G(d,p) was used to compute the MEP surface diagram of the DHA, which is depicted in **Figure 13**.

**Figure 13.** MEP diagram of the DHA calculated at DFT/B3LYP/6-311G(d,p) level

On the oxygen atoms in the anthraquinone group and the oxygen atom in the carboxylic acid moiety in the MEP diagram of DHA, some electron density was found. These red areas, which the high

electronegativity of oxygen caused, were the molecule's interaction sites for potential nucleophilic reactions. On the other hand, the phenolic proton and the proton linked to the carboxylic acid group were the electron-poor blue regions of DHA. Potential DHA interaction sites in electrophilic reactions were located in these blue regions.

3.5. ADMET predictions

A pharmacological molecule's creation must begin with the identification of ADMET properties. Most potential substances are rejected due to their unsuitable pharmacokinetic, druglikeness, etc. profiles.

When the physicochemical characteristics of the synthesized molecule DHA were assessed (**Figure 14**), its molecular weight was determined to be 372.33 g/mol. This value is within the limits of being a drug (150 g/mol <MW<500 g/mol). The TPSA value should be less than 140 Å² because TPSA values greater than 140 Å² make it more difficult to get through cell membranes [30]. DHA's TPSA value was determined to be 116.39 Å².

The dispersion between lipids and water is known as lipophilicity. Drug molecules must pass through numerous biological membranes, including the blood-brain barrier, the skin, and the gut, in order to reach their target areas. A chemical must therefore

dissolve at specific rates in both water and oil [31]. The many types of lipophilicity shown in **Figure 14** were discovered by various researchers using various mathematical equations. The mean lipophilicity (CLogPo/w) value of DHA was calculated to be 3.18.

One of the fundamentally important features in studies on drug development is solubility. This is because the drug's molecule must be soluble to reach its target. The maximum quantity of drug that can dissolve in the given mixture is known as logSw. When **Figure 14** is examined, it is seen that DHA resolution is moderately soluble according to the first two resolution types and poorly soluble according to the last resolution type.

A pharmacokinetic analysis of the compound DHA was also conducted. The liver contains crucial enzymes called cytochrome P450 (CYP) inhibitors that are involved in the metabolism of numerous drugs. Determining whether a specific substance will be a cytochrome P450 substrate is crucial. 2D6 and 3A4 are the two main isoforms in charge of drug metabolism. Five main cytochrome isoforms (CYP1A2, CYP2C19, CYP2C9, CYP2D6, and CYP3A4) are thought to be its estimated substrates. DHA inhibits the activity of CYP2C9 isoforms, as shown by **Figure 14**.

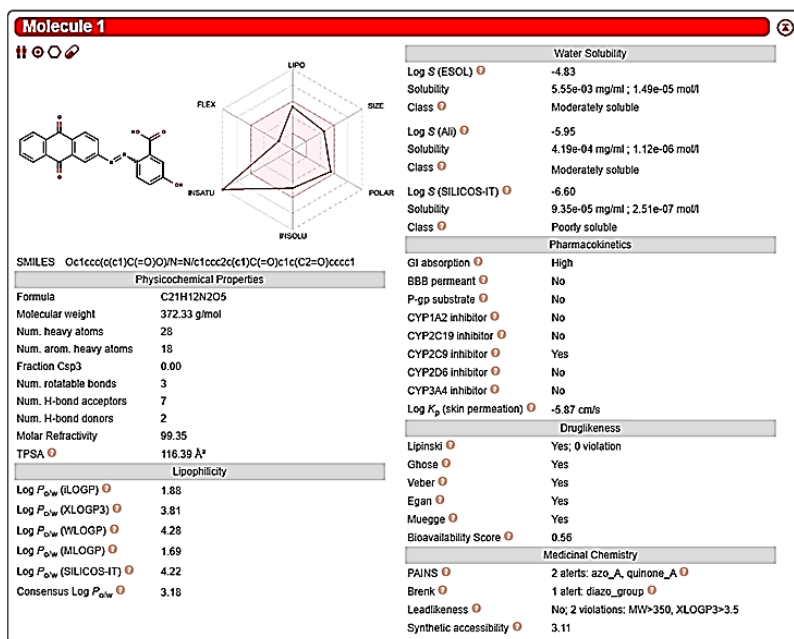


Figure 14. Physicochemical, lipophilicity, solubility, pharmacokinetics and druglikeness properties of the DHA

In **Figure 15**, DHA's BOILED-Egg graph, the ADME parameters GI (gastrointestinal absorption) and BBB (blood-brain barrier) were estimated. In this diagram, the white region contains potential GI absorption locations, while the yellow region has potential BBB permeability areas. Additionally, red dots (PGP-) show that P-gp is not a substrate, whereas blue

dots (PGP+) show that P-gp is an active substrate. A red dot (PGP-) indicates that the synthesized DHA compound is not a P-gp substrate, and its presence in the white region indicates that it is predicted to have high intestinal absorption and low brain permeability [32].

The DHA compound was assessed for pharmacological similarity using five different filters, including Lipinski (Pfizer), Ghose (Amgen), Veber (GSK), Egan (Pharmacia), and Muegge (Bayer), that are commonly employed by large pharmaceutical companies to enhance the quality of their proprietary drugs. According to all of the filters, it can be shown that the compound meets all requirements.

When DHA, a medication candidate chemical, is assessed using the PAINS, Brenk, Lead-like-

ness, and synthetic accessibility metrics, it is discovered that it provides two warnings in PAINS, one warning in Brenk, and two warnings in Lead-likeness. A measure of how simple it is to synthesize drug-like compounds is called synthetic accessibility. A scale from 1 (easiest to make) to 10 (very difficult to make) is used to rate synthetic accessibility. The DHA compound's synthetic accessibility score was determined to be 3.11.

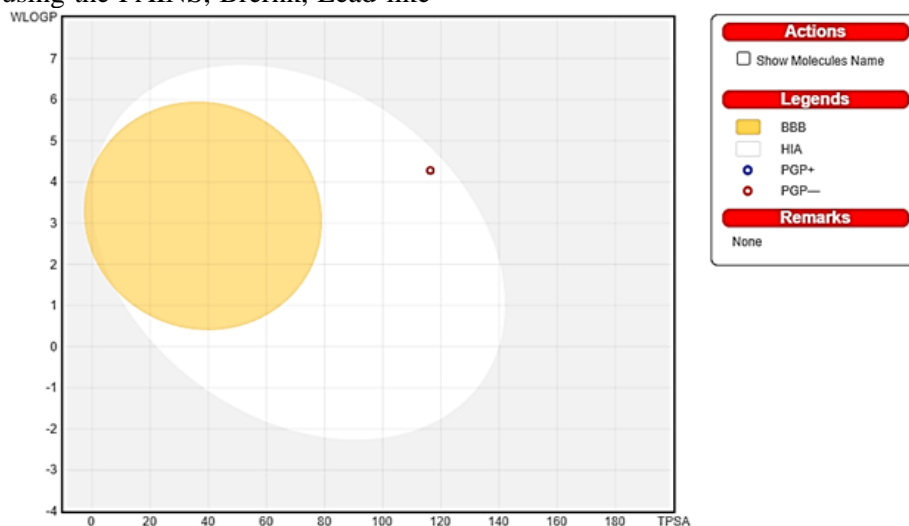


Figure 15. BOILED-Egg model of the DHA

The toxicity level and LD₅₀ number of DHA were calculated using the ProTox-II web server. DHA's LD₅₀ value was found to be 4000 mg/kg, and it had no immunotoxicity or mutagenicity. Additionally, the predicted toxicity classes for the compounds were established on the web server from worst to best,

ranging from 1 to 6. The DHA was in the fifth class, which was made up of substances with the highest LD₅₀ values due to its LD₅₀ value of 4000 mg/kg (**Figure 16**).

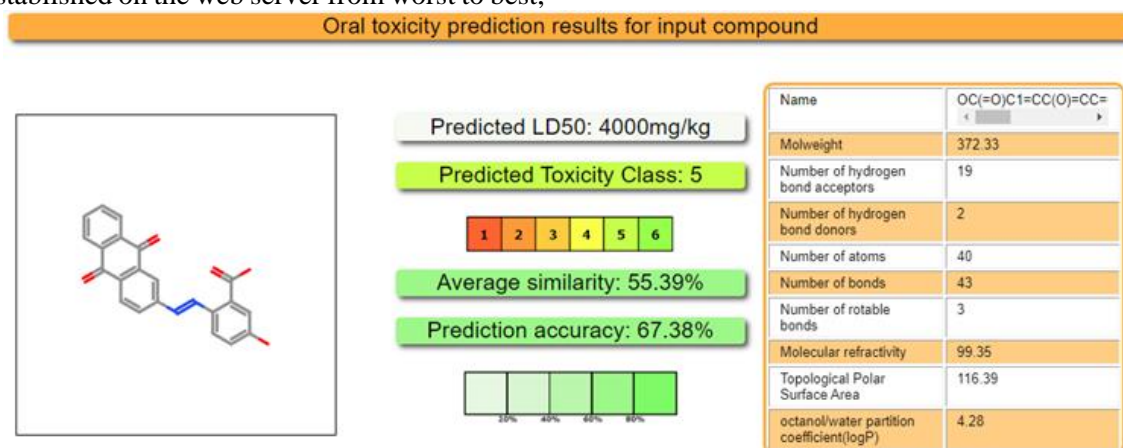


Figure 16. The predicted toxicity classes of the DHA

4. Conclusion and Suggestions

This research involved the synthesis of 2-[(9,10-dioxo-9,10-dihydroanthracen-2-yl)diazenyl]-5-hydroxybenzoic acid (DHA). HR-ESI-MS, FT-IR, ¹H-

NMR, ¹³C-NMR, and UV-vis spectroscopy were used to analyze the structure of the DHA. The DFT/B3LYP/6-311G(d,p) level was used to compute all of the DHA's spectral information. The characterization of the compound was helped by the fact that

all of the experimental results were in good agreement with the theoretical values. Additionally, DHA's global reactivity parameters and frontier molecular orbitals were determined. On the other side, it was found that DHA had a very high LD₅₀ value (4000 mg/kg). Thus, it was determined that the compound's toxicity was extremely minimal. The DHA computed all of the ADMET and drug similarity parameters within allowable ranges. In light of this, we believe that the DHA has the potential to be applied in more extensive studies in related areas.

Acknowledgment

Conflict of Interest Statement

There is no conflict of interest between the authors.

Statement of Research and Publication Ethics

The study is complied with research and publication ethics.

References

- [1] Y. Liu, M. S. T. Mapa and R. L. Sprando, "Anthraquinones inhibit cytochromes P450 enzyme activity in silico and in vitro," *J. Appl. Toxicol.*, vol. 41(9), pp.1438-1445, 2021.
- [2] H. Küçükbay, F. M. Parladi, F. Z. Küçükbay, A. Angeli, G. Bartolucci and C.T. Supuran, "Synthesis, antioxidant and carbonic anhydrase inhibitory properties of mono-peptide-anthraquinone conjugates," *Org. Commun.*, vol. 14, no.3, pp. 255-269, 2021.
- [3] U. Parladi, Ü. Yılmaz, S. A. A. Noma, B. Ateş and H. Küçükbay, "Synthesis of new anthraquinone compounds and evaluation of their considerable xanthine oxidase inhibitory activities," *ARKIVOC*, vol. 2022, pp. 158-167, 2022.
- [4] L. Dufossé, "Anthraquinones, the Dr Jekyll and Mr Hyde of the food pigment family," *Food Res. Int.*, vol. 65, Part B, pp. 132-136, November 2014.
- [5] J. Duval, V. Pecher, M. Poujol and E. Lesellier, "Research advances for the extraction, analysis and uses of anthraquinones: A review," *Indust. Crops and Products*, vol. 94, pp. 812–833, 2016.
- [6] S. C. Chien, Y. C. Wu, Z. W. Chen and W. C. Yang, "Naturally occurring anthraquinones: chemistry and therapeutic potential in autoimmune diabetes," *Hindawi Publishing Corporation Evidence-Based Complementary and Alternative Medicine*, pp. 1-13, March 2015.
- [7] F. Zhao, S. Zhao, J. T. Han, Y. F. Wang, Y. N. Wang and C. H. Wang, "Antiviral anthraquinones from the roots of *Knoxia valerianoides*," *Phytochem. Lett.*, vol. 11, pp. 57-60, March 2015.
- [8] J. Singh, Y. Hussain, S. Luqman and A. Meena, "Purpurin: A natural anthraquinone with multifaceted pharmacological activities," *Phytother. Res.*, vol. 35, no. 5, pp. 2418-2428, 2021.
- [9] A. Ntemafacka, R. V. Singh, S. Ali, J. R. Kuate and Q. P. Hassan, "Antiviral potential of anthraquinones from Polygonaceae, Rubiaceae and Asphodelaceae: Potent candidates in the treatment of SARS-COVID-19, A comprehensive review," *South African Journal of Botany*, vol. 151, Part A, pp. 146-155, December 2022.
- [10] A. Daina, O. Michielin and V. Zoete, "iLOGP: A simple, robust and efficient description of n-octanol/water partition coefficient for drug design using the GB/SA approach," *J. Chem. Inform. and Model.*, vol. 54, no. 12, pp. 3284-3301, 2014.
- [11] A. Daina, O. Michielin and V. Zoete, "SwissADME: A free web tool to evaluate pharmacokinetics, drug-likeness and medicinal chemistry friendliness of small molecules," *Sci. Rep.*, vol. 7, pp. 1-13, 2017.
- [12] M. Gökalp, B. Dede, Ç. Karabacak Atay and T. Tilki, "Triazole based azo molecules as potential antibacterial agents: Synthesis, characterization, DFT, ADME and molecular docking studies," *J. Mol. Struct.*, vol. 1212, pp. 128140, 2020.
- [13] B. Sezgin, B. Dede, Ç. Karabacak Atay and T. Tilki, "Synthesis, Characterization and Theoretical Calculations of a Novel Azo Derivative with In Vitro and In Silico Biological Studies," *Arab. J. Sci. Eng.*, vol. 46, pp. 5567–5581, 2021.
- [14] R. Sharma, R.K. Rawal, T.Gaba, N. Singla, M. Malhotra, S. Matharoo and T. R. Bhardwaj, "Design, synthesis and ex vivo evaluation of colon-specific azo based prodrugs of anticancer agents," *Bioorganic Med. Chem. Lett.*, vol. 23, pp. 5332-5338, 2013.
- [15] M. J. Frisch, G. W. Trucks, H. B. Schlegel, G. E. Scuseria, M. A. Robb, J. R. Cheeseman, G. Scalmani, V. Barone, G. A. Petersson, H. Nakatsuji, X. Li, M. Caricato, A. Marenich, J. Bloino, B. G. Janesko, R. Gomperts, B. Mennucci, H. P. Hratchian, J. V. Ortiz, A. F. Izmaylov, J. L. Sonnenberg, D. Williams-Young, F. Ding, F. Lipparini, F. Egidi, J. Goings, B. Peng, A. Petrone, T. Henderson, D. Ranasinghe,

- V. G. Zakrzewski, J. Gao, N. Rega, G. Zheng, W. Liang, M. Hada, M. Ehara, K. Toyota, R. Fukuda, J. Hasegawa, M. Ishida, T. Nakajima, Y. Honda, O. Kitao, H. Nakai, T. Vreven, K. Throssell, J. A. Montgomery Jr, J. E. Peralta, F. Ogliaro, M. Bearpark, J. J. Heyd, E. Brothers, K. N. Kudin, V. N. Staroverov, T. Keith, R. Kobayashi, J. Normand, K. Raghavachari, A. Rendell, J. C. Burant, S. S. Iyengar, J. Tomasi, M. Cossi, J. M. Millam, M. Klene, C. Adamo, R. Cammi, J. W. Ochterski, R. L. Martin, K. Morokuma, O. Farkas, J. B. Foresman, D. J. Fox, "Gaussian 09, Revision E.01," Gaussian Inc Wallingford CT, 2016.
- [16] R. Dennington, T. A. Keith, J. M. Millam, "GaussView, Revision 5.0.9," Semichem. Inc Shawnee Mission, KS, 2009.
- [17] A. D. Becke, "Density-functional exchange-energy approximation with correct asymptotic behavior," *Phys. Rev. A*, vol. 38, pp. 3098–3100, 1988.
- [18] C. Lee, W. Yang and R. G. Parr, "Development of the Colle-Salvetti correlation-energy formula into a functional of the electron density," *Phys. Rev. B*, vol. 37, pp. 785–789, 1988.
- [19] J. P. Merrick, D. Moran and L. Radom, "An evaluation of harmonic vibrational frequency scale factors," *J. Phys. Chem. A*, vol. 111, pp. 11683–11700, 2007.
- [20] R. Bauernschmitt and R. Ahlrichs, "Treatment of electronic excitations within the adiabatic approximation of time dependent density functional theory," *Chem. Phys. Lett.*, vol. 256, pp. 454–464, 1996.
- [21] M. E. Casida, C. Jamorski, K. C. Casida and D. R. Salahub, "Molecular excitation energies to high-lying bound states from time-dependent density-functional response theory: characterization and correction of the time-dependent local density approximation ionization threshold," *J. Chem. Phys.*, vol. 108, pp. 4439–4450, 1998.
- [22] N. M. O'Boyle, A. L. Tenderholt and K. M. Langner, "cclib: a library for package-independent computational chemistry algorithms," *J. Comput. Chem.*, vol. 29, pp. 839–845, 2008.
- [23] R. Ditchfield, "Molecular orbital theory of magnetic shielding and magnetic susceptibility," *J. Chem. Phys.*, vol. 56, pp. 5688–5691, 1972.
- [24] K. Wolinski, J. F. Hinton and P. Pulay, "Efficient implementation of the gauge-independent atomic orbital method for NMR chemical shift calculations," *J. Am. Chem. Soc.*, vol. 112, pp. 8251–8260, 1990.
- [25] A. Daina, O. Michielin and V. Zoete, "SwissADME: a free web tool to evaluate pharmacokinetics, drug-likeness and medicinal chemistry friendliness of small molecules," *Sci. Rep.*, vol. 7, no. 1, pp. 1–13, 2017.
- [26] P. Banerjee, O. A. Eckert, A. K. Schrey and R. Preissner, "ProTox-II: a webserver for the prediction of toxicity of chemicals," *Nucleic Acids Res.* (Web server issue 2018).
- [27] C. Li, T. Zhang, Z. Zeng, X. Liu, Y. Zhao, B. Zhang and Y. Feng, "A New Route to Indazolone via Amidation Reaction of o-Carboxyazobenzene," *Org. Lett.*, vol. 14, No. 2, pp. 479–481, 2012.
- [28] S. Riaz, A. Jabbar, Ambreen, S. Khaskheli, S. Sagheer and M. I. Choudhary, "Anthraquinone based anti-UV acid-azo dyes; a study of their synthesis, fastness, and UV-protection properties," *J. Mol. Struct.*, vol. 1272, 134219, 2023
- [29] H. F. Huang, W. Ma, B. T. Tang and S. F. Zhang, "Properties of a novel acid dye 1-amino-4-[(6-nitro-2-benzothiazolyl)amino]-9,10-anthraquinone-2-sulfonic acid with anti-UV capability," *Chin. Chem. Lett.*, vol. 21 pp. 417–420, 2010.
- [30] H. Pajouhesh and G. R. Lenz, "Medicinal Chemical Properties of Successful Central Nervous System Drugs, NeuroRx," *J. Am. Soc. Exp. NeuroTher.*, vol. 2, pp. 541–553, October 2005.
- [31] A. Mermer and S. Alyar, "Synthesis, characterization, DFT calculation, antioxidant activity, ADMET and molecular docking of thiosemicarbazide derivatives and their Cu II) complexes," *Chem.-Biol. Interact.*, vol. 351, 109742, 2022
- [32] A. Daina and V. Zoete, "A boiled-egg to predict gastrointestinal absorption and brain penetration of small molecules," *ChemMedChem*, vol. 11, pp. 1117–1121, 2016